Separation Science and Technology
Publication details, including instructions for authors and subscription information:
http://www.informaworld.com/smpp/title~content=t713708471

Determination of Filter Cake Properties by Nuclear Magnetic Resonance

Thomas Friedmann; Erich J. Windhab

To cite this Article Friedmann, Thomas and Windhab, Erich J.(1998) 'Determination of Filter Cake Properties by Nuclear Magnetic Resonance', Separation Science and Technology, 33: 14, 2221 — 2239
To link to this Article: DOI: 10.1080/01496399808545724
URL: http://dx.doi.org/10.1080/01496399808545724

SEPARATION SCIENCE AND TECHNOLOGY, 33(14), pp. 2221–2239, 1998

Determination of Filter Cake Properties by Nuclear Magnetic Resonance

THOMAS FRIEDMANN and ERICH J. WINDHAB*
INSTITUTE OF FOOD SCIENCE/FOOD ENGINEERING
SWISS FEDERAL INSTITUTE OF TECHNOLOGY (ETH)
8092 ZURICH, SWITZERLAND

ABSTRACT

Low resolution nuclear magnetic resonance (NMR) is used to investigate the porosity and permeability of filter cakes. Porosity is determined by free induction decay measurements of the fully saturated packings. NMR spin-lattice and spin-spin relaxation measurements were performed on the samples. It is shown that the permeability of the packed beds correlates strongly with the three material parameters of the sample: porosity ϵ and the relaxation time constants T_1 and T_2. All three parameters can be determined with a low resolution NMR spectrometer. Validation of the approach is achieved from flow experiments and analytical determination of porosity and permeability. After calibration, the new method allows an easy and rapid determination of filter cake properties under different process conditions. Changes of porosity and permeability of the filter cake during processing can be studied systematically. Filtration problems, such as compressibility of the filter cake or migration of small particles plugging the filter cake, can be analyzed with this method.

INTRODUCTION

Filtration processes for complex suspension systems forming compressible filter cakes (as found, for example, in the area of foods) are not easily described. Compressibility of the filter cake often results from such different compression mechanisms as slipping and rearrangement, breakage, or elastic deformation of the particles in the suspension forming the filter cake. The centrifugal force acting on the particles can lead to marked deformations,

* To whom correspondence should be addressed.

especially in filter centrifuges. Migration of small particles during the filtration process can lead to a high concentration of fine particles at the filter cloth, thus plugging the filter medium. Both compressibility and migration effects change the inner structure (pore size, porosity) of the filter cake significantly. A reduction of pore size will cause a decrease of permeability of the porous medium. Process parameters (pressure, centrifuge speed) and material parameters (particle size distribution, particle shape, compressibility) strongly influence permeability. The prediction of permeability is of great interest.

Nuclear magnetic resonance (NMR) has been used for the characterization of porous media in the past. Fluid distributions and pore size distributions have been measured by means of NMR techniques using various mathematical models for the interpretation of the relaxation data. Throughout the years, NMR has proved to be a fast and nondestructive method for determinations in porous materials. Most of the work has been done in the fields of geology and petroleum technology, where the fluid flow properties of porous media are also of great interest (1–4). In the food area, Hills (5) investigated the relationships between NMR water relaxation rates and water activity in several model porous materials and related the results to survival or growth of microorganisms in porous materials. Horsefield et al. (6) and La Heij et al. (7) used magnetic resonance imaging (MRI) for the determination of porosity profiles in filter cakes.

The possibility of estimating permeability from NMR data was suggested many years ago by Timur (8). He investigated the porosity ϵ and permeability k of sandstone samples and showed a strong correlation of log (k) with $\log(\epsilon^4\ T_1^2)$, where ϵ is the porosity of the sample and T_1 is the relaxation time. Other authors have since investigated the same problem for sandstones, rock cores, and synthetic porous samples (9–12).

In the present work, this approach was followed in order to verify the relationship between NMR relaxation times (T_1 and T_2) and permeability in several filter cakes (unconsolidated porous media). To the knowledge of the authors, there has not yet been a direct application of NMR techniques to filtration problems, such as estimation of filter cake permeability, involving compressible filter cakes. Permeability is determined from flow experiments through the packed beds in order to have the same flow conditions that occur during the filtration process. An established relationship would allow a fast and simple determination of permeabilities of packed beds under varying process conditions. As the permeability of compressible filter cakes during processing is not static, due to ongoing structural changes in the porous medium, a permeability estimation for a certain defined structure is difficult to make. However with the NMR method, a determination of filter cake characteristics is possible without disturbing the structure.

THEORY

Flow through porous media is described by Darcy's equation:

$$\frac{dV}{dt} = \frac{A\Delta p}{\eta RL} \tag{1}$$

Darcy's law predicts a direct proportionality of the pressure loss across the porous medium to the volume flow rate of the fluid (13). As shown in Eq. (1), Darcy's law is only valid for incompressible porous media (constant filter cake resistance R) and laminar ("streamline") flow conditions. The formation of turbulent eddies at higher Reynolds numbers causes a breakdown of the linearity between flow rate and pressure drop.

Flow conditions in a porous medium can be described with the dimensionless Reynolds number Re, given in Eq. (2), and the friction coefficient Λ. The latter has been used in several modified definitions by different authors. In this work the relationship proposed by Vorwerk and Brunn (14) is used, as shown in Eq. (3).

$$\mathrm{Re} = \frac{6 \cdot \rho \cdot \bar{v} \cdot R_h}{\eta} \tag{2}$$

$$\Lambda = \frac{36 \cdot R_h^2 \cdot \Delta p}{\eta \cdot \bar{v} \cdot L} \tag{3}$$

Permeability describes the ease with which a fluid passes through a porous medium. It is dependent on the porosity and structure of the filter cake and can be determined from flow experiments. The permeability k can be expressed as the reciprocal value of the filter cake resistance R as shown in Eq. (4).

$$k = 1/R \tag{4}$$

Caution has to be taken to evaluate permeability only from flow experiments in the laminar region (filtration processes mainly take place in this laminar flow region, due to small pore sizes). The friction coefficient Λ is shown to be constant (for a Newtonian fluid) up to Re numbers of approximately 10. The increase of Λ for $\mathrm{Re} \geq 10$ indicates turbulent flow in the porous medium.

In NMR spectroscopy the characteristic energy absorbed and reemited by nuclei (here protons) subjected to a static magnetic field and simultaneously irradiated with radio-frequency radiation is measured.

Magnetic field strengths commonly used in high resolution NMR are in the range of 1.4 to 14 Tesla, giving proton resonance frequencies of 60–600 MHz. With HR-NMR, individual atoms within a molecule can be probed (e.g.,

protons in different functional groups). Therefore, HR-NMR has become a valuable tool for studying molecules at the atomic level. Low resolution NMR uses magnetic field strengths in the range of 0.2 to 0.5 Tesla, giving proton resonance frequencies of 10–20 MHz. Low resolution NMR allows one to distinguish between different phases (e.g., solid–liquid) and is widely used in the food industry for quality control (e.g., solid fat content and water content).

The total magnetization of a very large number of spins has the magnitude M_0 and is aligned along the z-axis (at thermal equilibrium). The magnetic vector M_0, aligned with the static field, is disturbed by the radio-frequency pulse. In the form of an induced voltage in the receiver coil of the magnetic vector returning to its steady-state conditions, the response gives valuable information on the structural properties of the sample.

The decaying signal after the radio-frequency pulse is called the free induction decay (FID). The higher the concentration of atomic nuclei in the sample, the higher will be the signal intensity. Therefore, the initial amplitude of the signal in the FID can be used to measure the amount of a certain atomic nuclei in a sample.

Apart from the signal intensity, the relaxation of the amplitude as a function of time is characteristic for each sample.

The magnetic vector, as shown in Fig. 1 returns to equilibrium with a longitudinal (z-axis) and a transverse (x–y-plane) component. The longitudinal relaxation is also referred to as the spin-lattice relaxation time and is characterized by the time constant T_1. The transverse component is known as the spin-spin relaxation time and is characterized with the time constant T_2.

The magnetization intensity of the sample after the 90° radio-frequency pulse can be described by the following equations (15):

$$M(t)_{\text{longitudinal}} = M_0 \cdot (1 - \exp(-t/T_1)) \tag{5}$$

$$M(t)_{\text{transversal}} = M_0 \cdot \exp(-t/T_2) \tag{6}$$

The interaction of the spins with their surroundings causes the relaxation process. Since T_1 and T_2 describe different decay processes of the nuclear spins, and since NMR measurements always involve longitudinal and transverse relaxation, it is expected that a more complete description of the porous medium structure can be obtained by determining both the spin-lattice and the spin-spin relaxation time. During the T_1 relaxation process toward thermal equilibrium, energy in the form of heat is lost to the surroundings (e.g., pore surface) through molecular collisions. For this reason T_1 is called the spin-lattice relaxation time. Consequently, T_1 relaxation can be seen as an enthalpic process, whereas T_2 relaxation, which represents a mutual exchange of spin

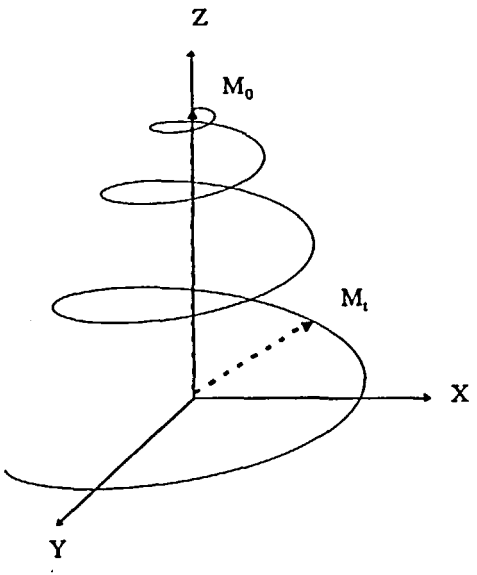

FIG. 1 Precession of magnetization vector after a 90° RF pulse back to equilibrium magnetization M_0. The magenetization vector precesses around the z-axis and at the same time returns to its equilibrium position along the z-axis.

energy, is regarded as an entropic process (16). From the physical point of view, the T_1 relaxation time is assumed to be correlated with the mean fluid distribution (e.g., mean pore size), whereas the T_2 relaxation time gives information on the amount of fluid in the porous medium. A paper on mechanisms of NMR relaxation of fluids in rocks has been presented by Kleinberg et al. (17). They found that the most important relaxation mechanisms arise from interactions with paramagnetic ions at the pore surfaces. The T_1/T_2 ratio was generally found to be significantly greater than 1.

Relaxation time constants can be measured with different pulse sequences. For liquids and other slowly decaying components, T_1 and T_2 are typically measured using the inversion recovery sequence and the Carr–Purcell–Meiboom–Gill (CPMG) sequence, respectively. In T_2 relaxation processes, the spin interactions cause the spins to precess at slightly different frequencies, and consequently lead to a destruction of their phase coherence. Two factors are mainly responsible for this dephasing: The intra- or intermolecular magnetic fields and the inhomogeneity of the static magnetic field. As the width of an NMR line depends on both factors, spin-spin relaxation times have to be measured by the spin echo technique that allows one to separate the two

processes. The dephasing caused by field inhomogeneity is "refocused" by the 180° pulse, and the NMR signal (spin echo) is detected and Fourier transformed to give a spectrum containing NMR lines whose amplitudes are independent of the field inhomogeneity. The mentioned NMR sequences have been described in detail in Ref. 18. Further background information on theory and applications to porous media can be found in Refs. 15 and 19–22.

EXPERIMENTAL

NMR experiments were performed using a Bruker Minispec NMS 120 spectrometer. The magnet had a field strength of 0.47 Tesla, giving a proton resonance frequency of 20 MHz. Measurements were performed at the magnet temperature of 40°C.

T_1 relaxation times were determined using the inversion recovery pulse sequence and subsequent monoexponential fitting of data points for T_1. For the T_2 relaxation times, the GPMG pulse sequence and subsequent monoexponential fitting was used.

Samples were inserted into the probehead in glass sample tubes of 10 or 18 mm inner diameter. The sample tubes were kept at 40°C for at least 30 minutes before measuring.

The particles forming the model filter cakes used in this work are listed in Table 1. The porosity of the packed beds was determined volumetrically.

For the NMR measurements, deionized water was used to fill the void pore volume. Special care was taken during sample preparation to avoid air bubbles in the porous medium.

TABLE 1
Particles Used for Model Filter Cakes

Code	Sample	Bead size (μm)	Packed bed porosity (—)
GK2000	Glass spheres	2000	0.394
GK1000	Glass spheres	1000	0.370
GK800	Glass spheres	800–1200	0.382
GK450	Glass spheres	450–500	0.368
GK355	Glass spheres	355–400	0.361
GK250	Glass spheres	250–400	0.400
GK100	Glass spheres	100–110	0.306
GK35	Glass spheres	35–50	0.394
GP250	Glass particles	250–400	0.503
KHSC	Kieselguhr Hyflo	10–100	0.870
LB250	Lignoblast (cellulose)	250–400	0.627

TABLE 2
Fluids Used for Flow Experiments

Fluid	Density (25°C) (kg/m^3)	Viscosity (25°C) (Pa·s)
Water	1000	0.001
Glucose syrup	1422	72
Polyethylene glycol (Hoechst PEG 35000):		
10% w/w solution	1016	0.023
25% w/w solution	1044	0.320

For flow experiments the particles were placed in a pressure filter. The filter diameter was 50 mm and the driving pressure gradient was achieved by superimposed air pressure up to 6 bar. Polyethylene glycol solutions (Hoechst, Germany) of different concentrations (10 and 25% w/w) and water were used as fluids.

The fluid mass flow rate was measured and the volume flow rate was calculated by consideration of the fluid density. The fluids used for the flow experiments are listed in Table 2.

Fluids of higher viscosity had to be used with some porous media in order to ensure laminar flow conditions. From the recorded data pressure drop and volume flow rate, the permeability k could be calculated according to Eqs. (1) and (4).

Flow experiments were performed at room temperature (25°C), and multiple measurements were made to reduce the influence of the random packing order of the porous media.

Another option used to achieve glass bead packing that keeps the same structure during all flow experiments is to fix the porous medium with a single-component instant adhesive prior to the flow measurements. The fixing technique was adapted from a method for dust filter cake conservation described in Ref. 23.

In addition to the glass beads model filter cakes, experiments with real systems have been carried out. The experiments presented here were done with ground coffee particles with a mean particle size of $x_{(50,3)} = 236$ μm. To avoid an additional influence of coffee extract components in the solution on the relaxation behavior, the ground coffee was extracted prior to NMR measurements. The extracted coffee was placed in sample tubes and the packed bed was saturated with deionized water. For compression experiments within the NMR spectrometer, a compression tool (plate) was used which allows one to apply a normal stress up to 10^5 Pa on the probe. T_1, T_2, and the sample height were measured at each stress level. The corresponding flow experiments for the coffee filter cakes were performed with a procedure

similar to the procedure previously described. In addition, the filter cake height was recorded with a CCD camera at the different pressure levels during filtration.

RESULTS AND DISCUSSION

Flow experiments through the different porous media yielded the volume flow rate as a function of the applied pressure. According to Darcy's equation, a direct proportionality exists in this relationship. In order to ensure laminar flow conditions in the porous medium, the Re number was calculated for the flow experiments according to Eq. (2). In Fig. 2 the friction coefficient (Eq. 3) versus Re number for a glass sphere packing (450–500 μm) shows the onset to turbulent conditions is at about Re = 10. This onset was also found in the same region (Re = 10–100) for the other packed beds. The friction coefficient is constant under laminar flow conditions for a Newtonian fluid. Therefore, the permeability of the packings was evaluated from data in the mentioned zone of constant friction coefficient. The permeabilities are listed in Table 3.

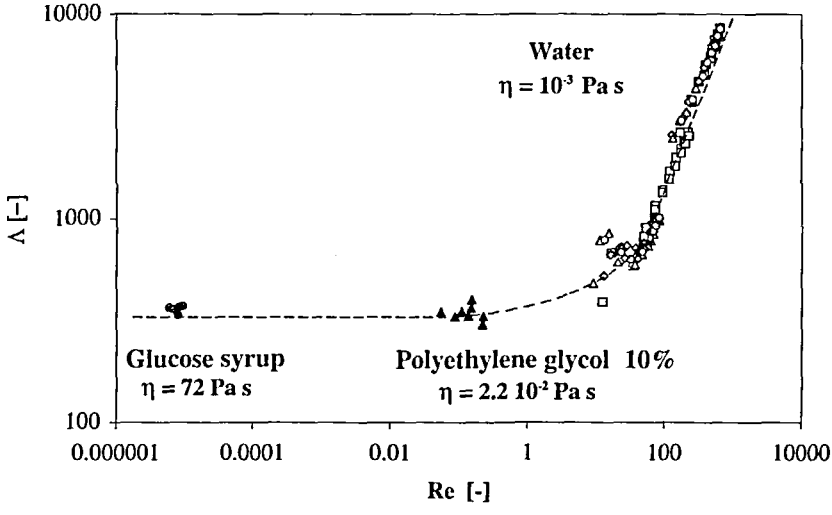

FIG. 2 Re–Λ relationship for glass bead packing (450–500 μm). From flow experiments in a pressure filter with fluids of different viscosity η to cover a larger Re number range. For a Newtonian fluid, Λ remains constant up to Re ≈ 10; increases of Λ at Re ≥ 10 indicate turbulent flow.

TABLE 3
Relaxation Time Constants T_1 and T_2 for Model Filter Cakes and Permeability k (determined with flow experiment)

Code	T_1 (ms)	T_2 (ms)	k (flow experiment) (m^2)
GK2000	2962	1250	5.86E-09
GK1000	2644	740	1.83E-09
GK800	1760	600	5.41E-10
GK450	1624	430	2.93E-10
GK355	892	232	6.82E-11
GK250	1012	183	1.13E-10
GK100	1671	150	1.02E-11
GK35	256	209	1.03E-12
GP250	1123	196	1.69E-10
KHSC	144	17	6.53E-14
LB250	380	176	2.65E-11

By comparing permeability and porosity of the same porous media, it is evident that porosity does not correlate with the permeability of a packed bed. As expected, the porosity of all glass sphere packings shows approximately the same value. The differences are mainly due to slightly different size distributions. However, permeability data of glass sphere packings show lower values with decreasing particle size. Kieselguhr (diatomite earth), which is often used in the food industry as a filter aid, has an extremely high porosity (around 85%). Such a high porosity value is achieved because of the inner porosity of kieselguhr particles. The characteristic shape, structure, and wide size distribution and incompressibility of kieselguhr also explain its good filter properties and its rather low permeability.

Measurement of the FID (free induction decay) signal in a water-filled porous medium can be used to determine the porosity of such filter cake systems. The maximum signal intensity (amplitude) is obtained when the radio frequency pulse is calibrated to rotate the sample magnetization by 90°. If the radio frequency pulse is consistent, the initial amplitude of the signal is directly proportional to the number of protons in the probe. For the calibration curve shown in Fig. 3, the initial amplitude which could be measured was used (after receiver dead time). The mean value of the data points in the sampling window (see Fig. 4) is the measured value used for calibration and measurement ("NMR signal"). The sampling window was chosen to be no longer than 0.2 ms. The delay after the 90° pulse was set to a minimum, so that the sampling window starts almost immediately after the receiver dead time. Assuming that the pores of the packing are completely filled with water, the calibrated FID signal yields the porosity.

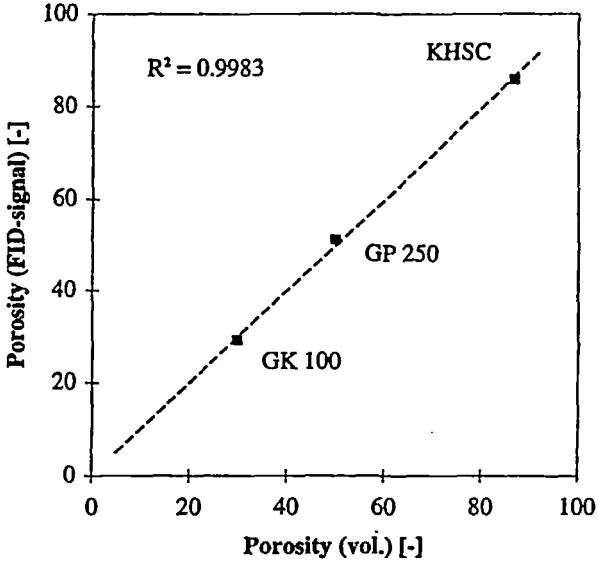

FIG. 3 Calibration of FID signal for porosity of porous medium. The FID signal can be essentially calibrated for porosity measurements with three calibration probes of known porosity.

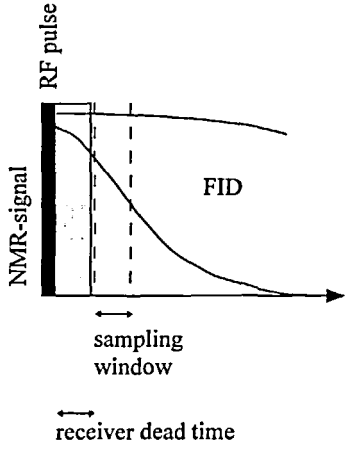

FIG. 4 FID signal and receiver dead time after RF pulse. No data acquisition is possible during receiver dead time. Data acquisition and averaging of the measured "NMR signal" takes place in the sampling window.

Attention must be paid so that the fluid signal does not decay substantially during the receiver dead time (RDT) of the NMR probehead, as shown schematically in Fig. 4.

If the receiver dead time of the probehead is too long for the analyzed system, there is the possibility of measuring the signal maxima between refocusing 180° pulses, as used for T_2 measurements. The signal amplitude at time t_0 (immediately after the RF pulse) can then be extrapolated. For the probes analyzed in this work, the receiver dead time posed no problem when measurement was with the 10 mm probehead, which has a lower RDT (8–9 μs) than the 18 mm probehead (15 μs).

All the T_1 measurements could be well approximated with a monoexponential fitting. Consistent with the varying pore structure of the packed beds, different relaxation time curves were obtained for the different systems. All relaxation measurement results for the model systems are summarized (T_1 and T_2) in Table 3. The T_1 results confirm the idea that the protons in the bulk fluid have a longer relaxation time than those near a pore wall. This indicates that porous media with longer relaxation times have a pore size distribution with larger pores than the media with short T_1 values.

The engineering aim of description and prediction of the permeability of the porous system from the porosity ϵ and the pore size, or the related particle size (average diameter d_p), has been elaborated by several authors. Some of the best known include the relationships of Blake–Kozeny (Eq. 7) and Rumpf–Gupte (Eq. 8) (24, 25):

$$k = \frac{d_p^2 \epsilon^3}{K(1 - \epsilon)^2} \tag{7}$$

$$k = \frac{d_p^2 \epsilon^m}{5.6} \tag{8}$$

In both equations the main structural parameters are the particle diameter d_p and the porosity, as well as a correction parameter (Kozeny constant $K = 150$; $m = 5.5$ in Rumpf–Gupte) which considers the tortuosity or pore structure of the filter cake.

When correlating the data obtained from NMR measurements (T_1, T_2) or porosity with permeability, the correlation coefficient is below 0.83 for single linear regressions, as shown in Fig. 5.

Combining the factors to a multiple linear regression with the two predictors T_1 and T_2, results in a much better correlation with the permeability. The statistical data are summarised in Table 4. T_1 and T_2 provide independent information. Relaxation involves two processes. Individual proton magnetic moments begin to lose synchronization (phase coherence) and also return

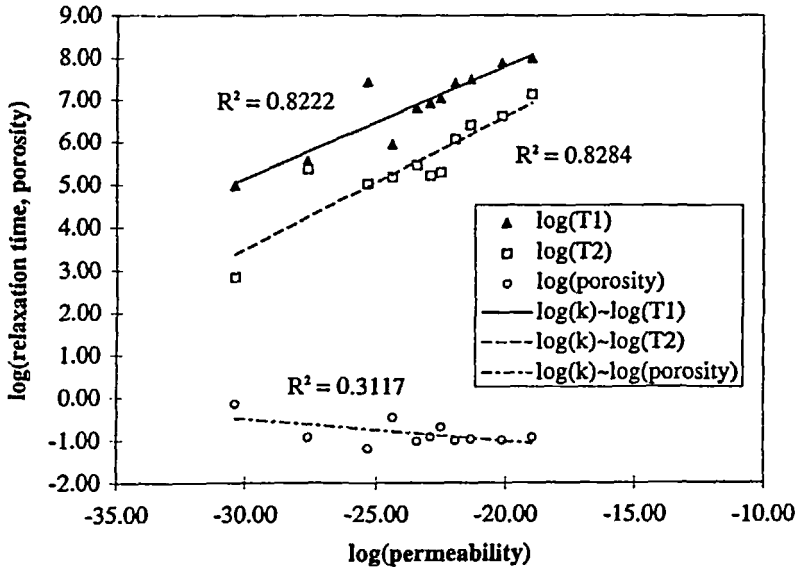

FIG. 5 Single linear regressions of structure data (T_1, T_2, porosity ϵ) with permeability determined from flow experiment.

TABLE 4
Statistical Data of Multiple Linear Regressions

Coefficients	Value	Standard error	t value	p value
		$\log(k) \sim \log(T_1) + \log(T_2)$		
Intercept	−46.6774	0.4626	−100.9081	<0.0001
$\log(T_1)$	2.7407	0.0811	33.8031	<0.0001
$\log(T_2)$	0.7609	0.1038	7.3296	<0.0001
Multiple R^2: 0.9321				
		$\log(k) \sim \log(T_1) + \log(T_2) + \log(\epsilon)$		
Intercept	−46.7366	0.2973	−157.2111	<0.0001
$\log(T_1)$	2.6260	0.0526	49.9397	<0.0001
$\log(T_2)$	1.5772	0.0837	18.8482	<0.0001
$\log(\epsilon)$	4.0672	0.2517	16.1595	<0.0001
Multiple R^2: 0.9721				

over time to their equilibrium position, precessing around the external magnetic field. These two relaxation processes occur with the characteristic exponential relaxation rates T_1 and T_2. It makes sense to use both relaxation time constants, T_1 and T_2, because each describes a different relaxation behavior of the fluid in the porous medium and, therefore, together they yield more information about the porous medium structure than does only one relaxation time. The two relaxation constants are characteristics of the environment surrounding the nuclei, and therefore they are the basis for distinguishing protons in different environments of porous structures. T_1 and T_2 can easily be measured with a low resolution NMR spectrometer, such as was used for these investigations. Thus, it offers a rapid and simple method for permeability estimation of filter cakes composed of different particles.

In Fig. 6 the experimentally determined permeability is compared to the permeabilities calculated from the Blake–Kozeny equation and the Rumpf–Gupte equation. The fitted permeabilities from NMR data (T_1, T_2) are also shown. From the correlation of NMR data and experimentally determined permeabilities, a relationship is derived which allows prediction not only of the permeabilities for packed beds with regular shapes (spheres) but also for more complex, real systems, such as kieselguhr. As shown in Fig. 6, for

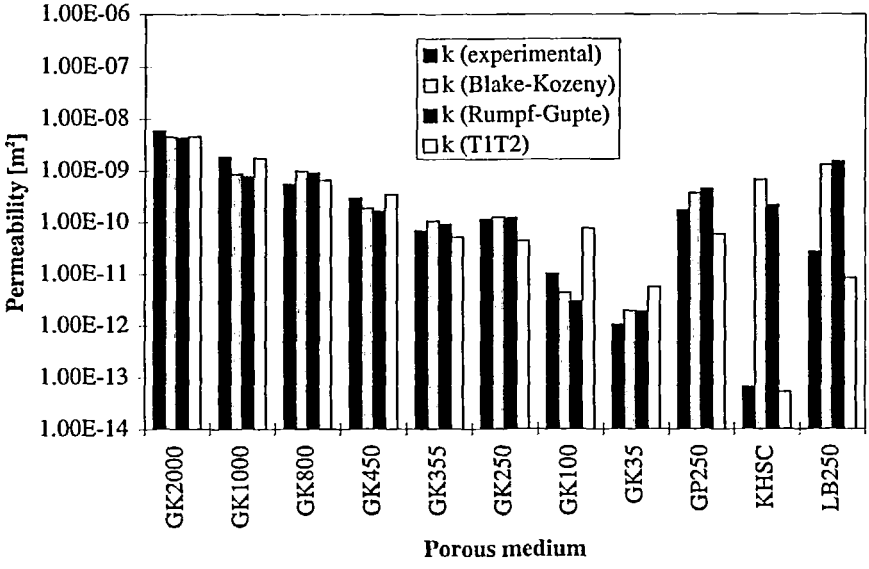

FIG. 6 Permeabilities of porous media determined by flow experiment, fitted from NMR-based relationship or Blake–Kozeny/Rumpf–Gupte relationships.

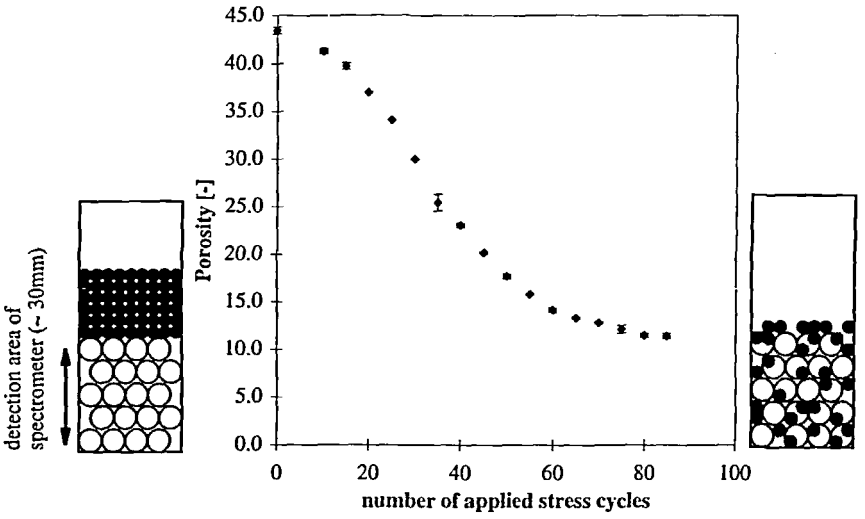

FIG. 7 Porosity changes in a porous medium caused by migration of smaller particles as measured with NMR (FID signal): 1000 μm glass spheres covered with a second layer of 100 μm glass spheres. The stress cycle was in the form of a vertical vibration imposed on the sample tube between each measurment.

porous media with particles differing the most from the spherical shape (e.g., Kieselguhr KHC and Lignoblast LB250), permeability is much better predicted by the T_1, T_2 method, than by the Blake–Kozeny and Rumpf–Gupte relationships, which contain particle diameter and porosity as predictors. This result seems evident, considering that there is a tortuosity or form factor in these equations. By measuring the relaxation behavior of a fluid in a porous medium, much of this structure information is included in the determined constants T_1 and T_2.

By adding the porosity as a third predictor to the multiple linear regression model, the correlation coefficient becomes even better and all three predictors are highly significant, as shown in Table 4. Measuring porosity in a conventional way is time-consuming. An alternative is the determination of the void volume fraction by means of NMR, as previously described. It would be possible to measure T_1, T_2, and porosity in succession in less than 10 minutes with the NMR method. The advantage of this nondestructive method is that the same sample can be measured several times (e.g., at different process stages). The results from a migration process are shown in Fig. 7. It is a common effect in filtration processes that finer particles migrate through the larger pores, leading to filter blocking. This phenomenon was simulated here

by covering a "filter cake" of 1000 μm glass spheres with a second layer of 100 μm glass spheres. By applying defined stresses (vertical vibration imposed on the sample tube between each measurement) on this model filter cake, migration was induced. The porosity of the packed bed was measured in the NMR spectrometer after every stress cycle. The FID signal related to porosity (see Fig. 3) was used for this measurement. Notice that the detection region of the spectrometer is only in the lower part of the sample tube, as indicated in Fig. 7. Similar experiments for quantification of permeability changes in the porous medium by measuring the relaxation times are possible. In addition, many other structural changes (e.g., compressible porous media) can be investigated with this method.

As real filter cakes are often compressible, the interest lies in the application of the NMR method for compressible filter cakes in order to describe the changes in permeability during compression. It was shown that the relaxation behavior is very sensitive to changes in the porous medium structure. Based on our relaxation time measurements of coffee particles, a significant change in T_1 and T_2 can be observed with ongoing compression of the packed bed. As shown in Fig. 8, the relaxation time decreases with higher applied stresses on the packing. This observation is consistent with the experimental findings

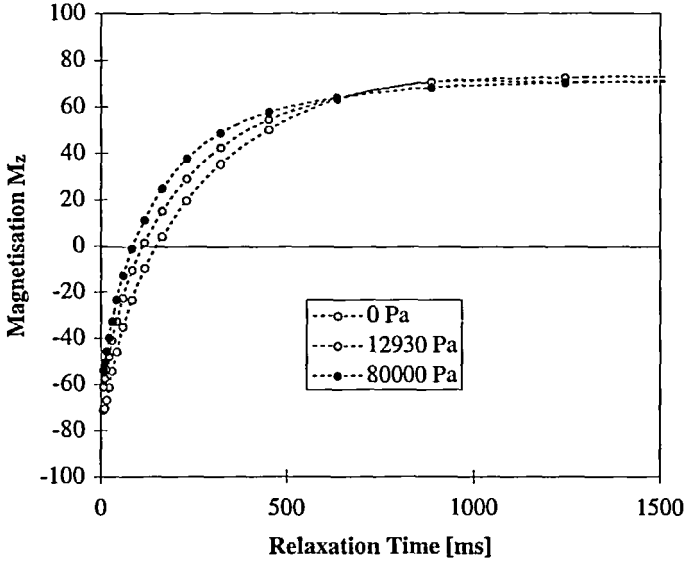

FIG. 8 T_1 evolution of packed bed of coffee particles ($x_{(50,3)}$ = 236 μm) with increasing normal stress on the packed bed (compression of filter cake).

of the model particles where lower relaxation times were measured in porous media systems with decreasing pore size distributions. During compression of a filter cake, the deformation of the packed bed leads to a pore size distribution shifted to smaller diameters and a decrease in the porosity. In Fig. 9 the measured relaxation time constants and the porosity at the different pressure levels for the packed bed of coffee particles are summarized. The circles in the diagram denote the experimental permeability values for the same system determined by a flow experiment. The triangles indicate the fitted values for permeability that were calculated from the relationship determined by multiple regression. Currently, compression tests in a NMR spectrometer allow a maximum normal stress of 10^5 Pa to be applied. However many separation processes take place at higher pressures. Extrapolation of the NMR-based relationship can give an estimate of permeability at higher pressure levels. Such an extrapolation is shown in Fig. 10. It is evident that with further extrapolation the accuracy will be reduced. Deviations from the experimental values are, however, within a reasonable range (15%) when extrapolating up to a pressure of 5 bar. Considering that it is possible to measure the permeability of a product system (e.g., with different particle size and particle shape), once calibration is done the structure characterization of filter cakes by NMR

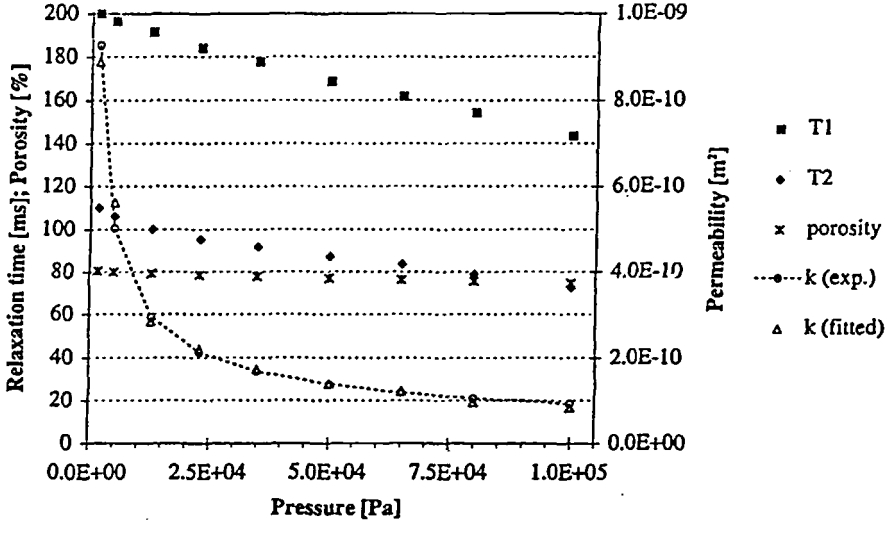

FIG. 9 Relaxation time constants (T_1, T_2), porosity, and permeability (experimental data and values fitted from multiple regression) for a packed bed of coffee particles at increasing normal stress levels.

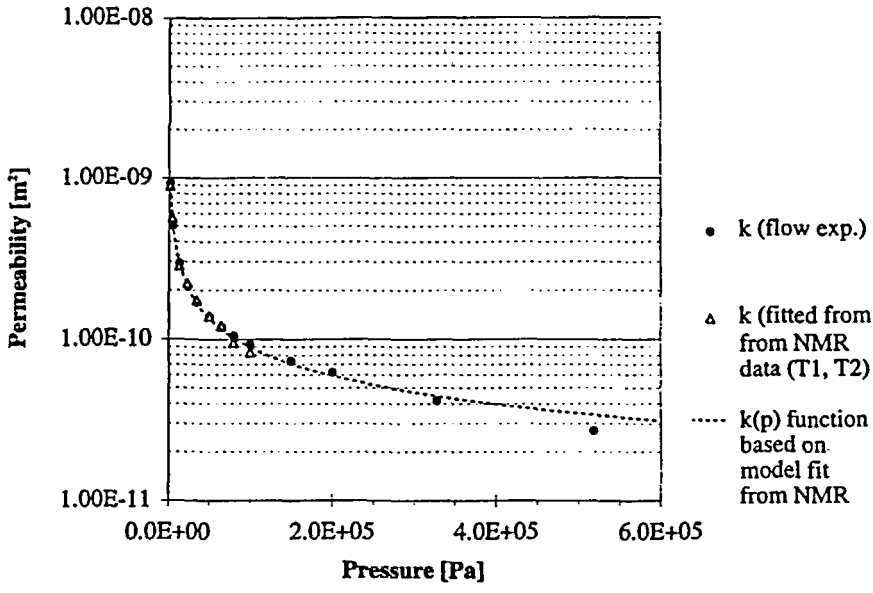

FIG. 10 Permeability as a function of applied pressure for a packed bed of coffee particles.

offers a new method for systematic investigations of filter cake compressibility and permeability as a function of material and process parameters.

CONCLUSIONS

The permeabilities of different porous media models were determined experimentally. From the same porous media, spin-lattice relaxation time (T_1) and spin-spin relaxation time (T_2) were measured in a low resolution (20 MHz) NMR spectrometer.

It was found that a prediction of permeability of such porous systems is possible from measurements of the relaxation time constants T_1 and T_2. The relaxation behavior of fully water-saturated porous media seems to contain much structural information about the packed bed. By the use of different NMR measurement techniques, it is also possible to extract specific structure information (e.g., pore size distribution). The correlation of NMR data to a specific structure property is not always evident. Where the FID signal can be clearly correlated to the void volume fraction or porosity, T_1 and T_2 are constants describing the exponential relaxation behavior of the fluid in the

pore volume. Mathematical models of the pore structure are necessary in order to extract pore size or even pore size distributions from relaxation data, as shown in other research. In this work, emphasis was placed on a relationship based on NMR measurements in order to characterize the porous medium with respect to fluid flow (permeability) through a system as it occurs in filtration processes. The authors see the advantage of this method in the relatively fast and nondestructive determination of filter cake properties. Because of the noninvasive characteristic of this method, an examination of the same sample at different process stages is possible. The determination of T_1 and T_2 at different compression stages allows one to describe the deformation behavior of the sample and the evolution of permeability with increasing stress on the filter cake.

The results presented here for cellulose/lignin particles (Lignoblast) as a model filter cake and with coffee as a real system indicate that the method is suitable for application to more complex systems. Once the calibration of NMR data has been done for a certain material (e.g., coffee), the NMR technique can be used as a quality control technique for the primary product (ground coffee) prior to extraction/filtration, as well as for the systematic investigation of the influence of material and process parameters on filter cake properties. The prediction of filterability can be of great help in many technical applications.

SYMBOLS

A	filter area (m^2)
d_p	particle diameter (m)
dV/dt	volume flow rate (m^3/s)
ϵ	porosity (—)
η	viscosity (Pa·s)
k	permeability (m^2)
K	constant in Eq. (7) (Kozeny constant)
L	filter cake height (m)
Λ	friction coefficient (—)
m	constant in Eq. (8)
$M_{(t)}$	magnetization at time t
M_0	equilibrium magnetization
Δp	pressure difference (Pa)
R	filter cake resistance ($1/m^2$)
ρ	density (kg/m^3)
Re	Reynolds number (—)
RF	radio frequency (Hz)
R_h	hydraulic radius (m)

T_1 spin-lattice relaxation time (ms)
T_2 spin-spin relaxation time (ms)
$\bar{v}$ average velocity (m/s)

REFERENCES

1. G. C. Borgia, R. J. S. Brown, and P. Fantazzini, *J. Appl. Phys.*, *79*, 3656–3664 (1996).
2. M. B. Carr, R. Ehrlich, M. C. Bowers, and J. J. Howard, *J. Pet. Sci. Eng.*, *14*, 115–131 (1996).
3. S. Davies, M. Z. Kalam, K. J. Packer, and F. O. Zelaya, *J. Appl. Phys.*, *67*, 3171–3176 (1990).
4. H.-K. Liaw, R. Kulkarni, S. Chen, and A. T. Watson, *Am. Inst. Chem. Eng. J.*, *42*, 538–546 (1996).
5. B. P. Hills, C. E. Manning, Y. Rigde, and T. Brocklehurst, *J. Sci. Food Agric.*, *71*, 185–194 (1996).
6. M. A. Horsefield, E. J. Fordham, C. Hall, and L. D. Hall, *J. Magn. Reson.*, *81*, 593–596 (1989).
7. E. J. La Heij, P. Kerkhof, K. Kopinga, and L. Pel, *AIChE J.*, *42*, 953–959 (1996).
8. A. Timur, *J. Pet. Technol.*, pp. 775–786 (1969).
9. U. Bilardo, G. C. Borgia, V. Bortolotti, P. Fantazzini, and E. Mesini, *J. Pet. Sci. Eng.*, *5*, 273–283 (1991).
10. W. E. Kenyon, *Nucl. Geophys.*, *6*, 153–171 (1992).
11. B. Issa and P. Mansfield, *Magn. Reson. Imaging*, *12*, 213–214 (1994).
12. A. H. Thompson et al., *J. Appl. Phys.*, *65*, 3259–3263 (1989).
13. H. P. G. Darcy, *Les Fontaines publiques de la ville de Dijon*, Victor Dalmont, Paris, 1856.
14. J. Vorwerk and P. O. Brunn, *J. Non-Newtonian Fluid Mech.*, *51*, 79–95 (1994).
15. H. Todt, *Minispec Application Training Course*, 1997.
16. S. W. Homans, *A Dictionary of Concepts in NMR*, Clarendon Press, Oxford, 1995.
17. R. L. Kleinberg, W. E. Kenyon, and P. P. Mitra, *J. Magn. Reson.*, *108*, 206–214 (1994).
18. S. W. Young, *Magnetic Resonance Imaging: Basic Principles*, 2nd ed., Raven Press, New York, NY, 1984.
19. M. P. Hollewand and L. F. Gladden, *Chem. Eng. Sci.*, *50*, 309–326 (1995).
20. P. J. Hore, *Nuclear Magnetic Resonance*, *Vol. 32*, Oxford Science Publications, Oxford, 1995.
21. K. Munn and D. M. Smith, *J. Colloid Interface Sci.*, *119*, 117–126 (1987).
22. W. M. Ritchey, *Appl. Spectros. Rev.*, *29*, 233–267 (1994).
23. E. Schmidt, *Powder Technol.*, *60*, 173–177 (1990).
24. B. R. Bird, W. E. Stewart, and E. N. Lightfoot, *Transport Phenomena*, Wiley, New York, NY, 1960.
25. H. Rumpf and A. R. Gupte, *Chem.-Ing.-Tech.*, *43*, 367–375 (1971).

Received by editor September 29, 1997
Revision received February 1998